Threshold photoelectron source for the study of low-energy electron scattering: Total cross section for electron scattering from krypton in the energy range from 14 meV to 20 eV

M. Kurokawa,[1] M. Kitajima,[1,*] K. Toyoshima,[1] T. Odagiri,[1] H. Kato,[2] H. Kawahara,[2] M. Hoshino,[2] H. Tanaka,[2] and K. Ito[3]

[1]*Department of Chemistry, Tokyo Institute of Technology, Tokyo 152-8551, Japan*

[2]*Department of Physics, Sophia University, Tokyo 102-8554, Japan*

[3]*Photon Factory, Institute of Materials Structure Science, Tsukuba 305-0801, Japan*

(Received 6 October 2010; published 13 December 2010)

An experimental technique for the measurement of the total cross section for electron scattering from atoms and molecules at high resolution is described. The total cross sections for electron scattering from Kr in the energy range from 14 meV to 20 eV obtained with the technique are also reported. The present technique employs a combination of the penetrating field technique and the threshold photoionization of rare-gas atoms using synchrotron radiation as an electron source in order to produce a high-resolution electron beam at very low energy. The characteristics of the electron sources were determined by measuring the ionizing photon energy dependence of photoelectron yield. Absolute total cross sections for electron scattering are obtained by the attenuation method. The measured absolute values of the total cross sections for electron scattering from Kr agree with those obtained by other groups down to 175 meV, above which several experimental works have been reported. Below 175 meV, the present results generally agree with theoretical cross sections down to 14 meV. The resonant structures in the total cross sections due to Kr^- $(4p^5 5s^2\,{}^2P_{3/2})$ and the Kr^- $(4p^5 5s^2\,{}^2P_{1/2})$ Feshbach resonances are also reported. The resolution of the present setup has been estimated from a fit of the measured profile of the Kr^- $(4p^5 5s^2\,{}^2P_{3/2})$ resonance by the theoretical curve obtained from the resonant scattering theory.

DOI: 10.1103/PhysRevA.82.062707 PACS number(s): 34.80.Bm, 52.20.Fs

I. INTRODUCTION

The scattering of low-energy electrons by atoms and molecules has been the subject of extensive experimental and theoretical investigations. The cross-section data concerning electron-atom or -molecule scattering are of great importance in understanding fundamental physics of the electron collisions and applications such as electron-driven processes in the Earth and planets' phenomena, radiation chemistry, gaseous discharges, plasmas, and so on. A variety of quantum phenomena, such as the Ramsauer-Townsend effect [1,2] and resonant behavior [3,4], were observed in the scattering of low-energy electrons by atoms and molecules. Up to now, most of the experimental studies on low-energy electron collision in the gas phase have been performed with the technique using a hot-filament electron source followed by an electrostatic monochromator. The typical electron energy width is in the range of 30–150 meV. In a very few cases, extremely high resolution up to 7 meV has been achieved [5]. Another technique using time-of-flight energy selection with pulsed electron beams has been proposed [6,7]. In this method, the resolution of the electron beam is energy dependent and can be as high as 5 meV at low incident energies (<250 meV).

An alternative method for reaching even higher resolutions is through near-threshold photoionization of atoms by making use of a photoelectron source. Photoelectron sources for electron-atom collision experiments have been used by a few groups since the pioneering work of Gallagher and co-workers utilizing photoelectrons produced from the photoionization of a Ba atom by cw He-Cd laser [8,9]. They studied elastic electron scattering from several atoms at an overall resolution of 2 meV. Chutjian and co-workers employed monochromatized radiation from a Hopfield continuum light source to generate photoelectrons of energies in the range of 1–200 meV and studied electron attachment with molecules below 200 meV with energy resolutions of 4–6 meV [10,11].

Hotop and co-workers developed the laser photoelectron attachment (LPA) method and extended the energy range down to the sub-meV region with extremely high energy resolution [12,13]. Highly resolved attachment yield spectra obtained for anion formation over the typical energy range 0.2-200 meV under sub-meV resolution were obtained by the LPA method [14–16]. On the other hand, formation of very-low-energy electron beams was not the issue in these electron-attachment experiments. Recently, Hotop and co-workers have applied their laser photoionization technique to produce a high-resolution electron beam, energy width typically from 4 to 11 meV, in the energy range of 10 to 20 eV for electron scattering experiments [17–21]. Elastic and inelastic differential cross sections for electron scattering from rare-gas atoms and N_2 have been obtained in these studies.

Measurements of the total cross section for electron scattering from various molecules at very low energies have been carried out by Field and Ziesel with co-workers [22–26]. In their technique, the photoelectrons from the photoionization of Ar with monochromatized synchrotron radiation (SR) tuned at the autoionization resonance Ar^{**} $(4p^5\,{}^2P_{1/2})$ $11s'$ just above the ionization threshold with the photon bandwidth of 1–4 meV are extracted by a weak constant electric field applied across the photoionization region and formed into a beam by a four-element lens system. Total cross sections (including backward scattering cross sections) for electron scattering from several molecular targets at very low energies in the cold electron collisions regime, where the de Broglie wavelength of an electron becomes much lager than the typical

*mkitajim@chem.titech.ac.jp

size of target, have been reported by this group [24–26]. Since only the group of Field *et al.* has realized a method of obtaining the total cross sections for electron scattering from molecules in the cold electron collision regime, most of the existing total cross-section data below a few hundred meV have been obtained by this group. However, in their recent report on NH_3, H_2S, and OCS, they found that a number of serious discrepancies exist for the total cross sections among the data in the literature at impact energies below a few eV [26].

One of the difficulties in the high-resolution, low-energy electron collision experiments employing photoelectron sources is the trade-off problem between the resolution and the intensity of the electron beam. The electric field applied across the photoionization region degrades the electron-beam energy resolution. Therefore, it is necessary to narrow the size of the photon beam used in the photoionization process, which in turn means reducing the intensity of the photon beam and, hence, reducing the intensity of the electron beam. In addition, narrowing the photon beam requires highly accurate optical alignment. In order to meet these demands, the experimental setup of Field and co-workers has been fixed on a special beamline constructed for the particular purpose [25].

Here we present a new method for producing an electron beam at very low energy including cold electron collision regime for measuring the total cross section for electron scattering from atoms and molecules, employing a photoelectron source. The method overcomes the trade-off problem between the resolution and the intensity of the electron beam from the photoelectron source by applying in combination the threshold photoionization of atoms and the penetrating field technique [27].

We have measured total cross sections for electron scattering from Kr in the energy range from 14 meV to 20 eV in order to demonstrate the capability of the present apparatus. Up to now, several experimental groups have investigated total cross sections of electron scattering from rare gases in the low-energy region. The total cross-section curve for electron scattering from Kr shows the well-known Ramsauer-Townsend minimum at around 0.7 eV, with a local value less than 1×10^{-20} m^2 and a maximum at around 12 eV with a value greater than 25×10^{-20} m^2 [28–32]. In general, the total cross-section curves of previous experiments agree reasonably well [28–32]; hence, the total cross-section measurements of Kr may serve as a benchmark for the new setup. In addition, the only cross section obtained below 175 meV has been reported by Gus'kov *et al.* [33]; their values disagree with others at higher energies. Further measurements on the total electron scattering cross sections from Kr are necessary for the low-energy electron collisions, especially in the very-low-energy region down to the cold electron collision's regime.

Here we also report the resonant structures due to the Kr^- $(4p^5 5s^2\,^2P_{3/2})$ and the Kr^- $(4p^5 5s^2\,^2P_{1/2})$ Feshbach resonances observed in the total cross-section curve. The structures due to the resonances have been extensively studied by transmission measurements [34–36] and angular differential cross-section measurements [21,37–40]; however, total cross sections for these resonances have not yet been reported.

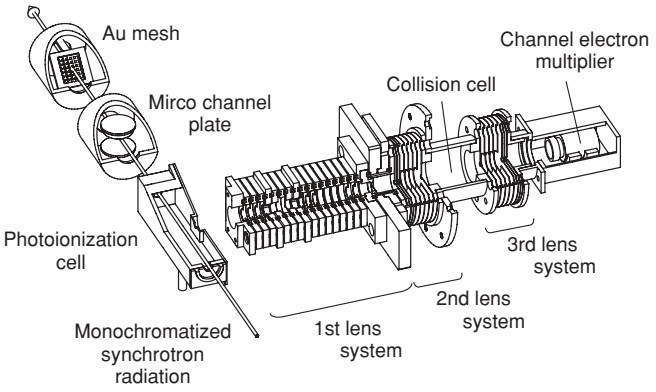

FIG. 1. Overview of the present experimental system. The system consists of an electron scattering apparatus with a photoionization cell, a microchannel plate to measure photoion yield spectra, and an Au mesh to monitor the flux of the monochromatized SR. The monochromaitzed SR is focused onto the center of the photoionization cell filled with argon atoms for producing photoelectrons.

II. EXPERIMENTAL

A. The experimental system

An overview of the experimental setup is shown in Fig. 1. The setup consists of an electron scattering apparatus with a photoelectron source, an Au mesh monitor, and a microchannel plate (MCP). The electron scattering apparatus consists of a photoionization cell, three electrostatic lens systems, a collision cell, and a channel electron multiplier. The experiment has been carried out at the beamline 20A of the Photon Factory, KEK, in Japan. A 3-m normal-incidence monochromator equipped with a 2400 lines/mm grating is installed in this beamline [41].

The monochromatized SR tuned just at the first ionization threshold of Ar (15.760 eV) was focused on the center of the photoionization cell, filled with argon atoms. The threshold photoelectrons produced are extracted by a weak electrostatic field formed by the penetrating field technique and focused onto the entrance of a lens systems of the electron scattering apparatus. The electrons are conducted into the second lens system and transmitted to the collision cell filled with target gas. The electrons passing through the cell without any collision with the target are refocused by the third lens system and detected by a channel electron multiplier. The counting rates of the detected electrons in the presence and absence of target gas are converted to the total cross section for electron scattering according to the attenuation law, as is described in Sec. II D. The whole of the photoionization cell and scattering apparatus are placed inside the double μ-metal shields to attenuate Earth's magnetic field. The stray magnetic field is estimated to be less than 10^{-7} T, which is sufficiently small not to interact with the lowest-energy electron in the present experiment. The flux of the ionizing photon beam was monitored by the Au mesh. The MCP was set in order to measure the photoion yield spectra of Ar during the tuning of the electron scattering apparatus. The vacuum chamber containing the scattering apparatus, the photoionization cell, the Au mesh, and the MCP is pumped by three 400 L s^{-1} turbopumps. The typical operating and the

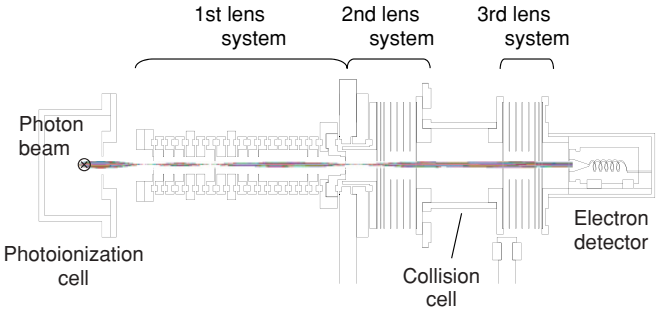

FIG. 2. (Color online) Cross section of the apparatus used in the measurement of the total electron scattering cross sections. A monochromatic photon beam at the first ionization threshold of Ar 15.760 eV is introduced into the photoionization cell. The photoelectrons are collected by the penetrating field from the the first lens system and formed into a beam. The electron beam is tuned by the second lens system and focused onto the collision cell filled with target gas. The transmitted electrons are accelerated by the third lens system and detected by a channel electron multiplier. The results of the electron trajectory calculation at a collision energy of 0.1 eV are also shown.

background pressure in the chamber are about 1.0×10^{-3} and 1.0×10^{-5} Pa, respectively.

B. Electron scattering apparatus utilizing the penetrating field technique

A cross section of the electron scattering apparatus is shown in Fig. 2. In the present setup, a photoelectron source of a different kind is employed. The method combines threshold photoionization of atoms and the penetrating field technique. The penetrating field technique developed by Cvejanović and Read [27] utilizes the very weak field in the photoionization region formed by an extraction electrode penetrating through a screening electrode. The penetrating field forms a saddle point in the potential distribution that has the effect of focusing and enhancing the extraction efficiency of photoelectrons of particular energy. By tuning the penetrating field, only very-low-energy photoelectrons can be extracted from the photoionization region and focused onto the entrance of the lens system, while the energetic photoelectrons rapidly diverge [27,42,43].

In the present apparatus, the photoionization cell and the first electrostatic lens system serve as the photoelectron source. The first lens system consists of an extraction electrode to produce a penetrating field in the photoionization cell, a pair of slits with holes of 0.5 mm diameter, and a multielement lens system which has a strong aberration. The wall of the photoioniation cell, which has a 3-mm-diameter hole for the entry of the extracting field, acts as a screening electrode. The typical potential on the extraction electrode is 5 V, which results in an electric field of about 0.02 V/cm in the center of photoionization region. The advantage of this first lens system is that the paths of the transmitted electrons are very well defined so that unwanted electrons are strongly suppressed and, therefore, energy selectivity is very high.

The electron beam focused on the last slit of the first lens system was then energy adjusted and led into the collision cell by the second lens system. The length of the collision cell is 30.5 mm and the diameters of both entrance and exit holes are 2 mm. After passing through the collision cell the electron beam was accelerated by the third lens system and focused onto the entrance of the channel electron multiplier. The use of the independent third lens systems enables the measurement in a wide energy range from the energy region of the cold electron collision to a few tenths of electron volts.

The present method utilizing the penetrating field technique has an advantage of weakening electrostatic field for the collection of the photoelectrons in the photoionization region. Since the electric field applied across the photoionization region degrades the energy resolution of the electron beam, a narrow photon beam is necessary for the formation of a high-resolution electron beam. The typical size of the photon beam and the electric field strength applied to the photoionization region in the case of the experimental setup of Field *et al.* were a strip of thickness of 10 μm and 0.2–0.4 V/cm, respectively [24]. However, narrowing the size of the photon beam may reduce the intensity of the photoionization radiation and also demands a highly accurate optical alignment of the experimental setup. In the present case, the electric field at the center of the photoionization region was reduced to about 0.02 V/cm to allow for enough collection of photoelectrons by utilizing the penetrating field technique. The size of the photon beam was 1 mm in diameter.

Doppler broadening of the threshold photoelectrons is very small in the present case. The resolution due to the Doppler effect is estimated to be less than 0.1 meV, given by

$$0.723(ET/M)^{1/2}, \tag{1}$$

where E is the energy of the photoelectron in electron volts, T is the temperature of the photoionization cell in Kelvin and M is the mass of argon atom in atomic units [44].

C. Energy selectivity for the photoelectron source

The energy selectivity of the present setup for the photoelectrons can be estimated from the photoelectron yield as a function of the ionizaiton photon energy, that is, electron yield spectrum. Figure 3 shows the electron yield spectrum of Ar obtained at a typical experimental condition around the ionization threshold together with the photoion yield spectrum. Strong peaks of the electron yield spectrum appear only when the photon energy crosses each of the ionization thresholds of Ar. The typical count rate of the electron at the $Ar^+ {}^2P_{3/2}$ threshold was 10 000 counts per second.

The structures in the photoion yield spectrum correspond to high-lying neutral Rydberg states converging to the $Ar^+ {}^2P_{1/2}$ ion state, that is, autoionizing states [45]. These Rydberg states can decay to the lower-lying $Ar^+ {}^2P_{3/2}$ ionic state, resulting in the emission of electrons of kinetic energy equal to the excess energy of the Rydberg level above the $^2P_{3/2}$ ionization threshold. Detection or suppression of these energetic electrons is a good test of the performance of the present setup as an electron monochromator [43]. Clearly from Fig. 3, energetic electrons produced by the autoionization of the Rydberg series of Ar^{**} $(4p^5 {}^2P_{1/2})$ ns' $(n \geqslant 12)$ are strongly discriminated. As shown in Fig. 3(b), contribution from the Rydberg state of Ar^{**} $(4p^5 {}^2P_{1/2})$ $11s'$ is relatively

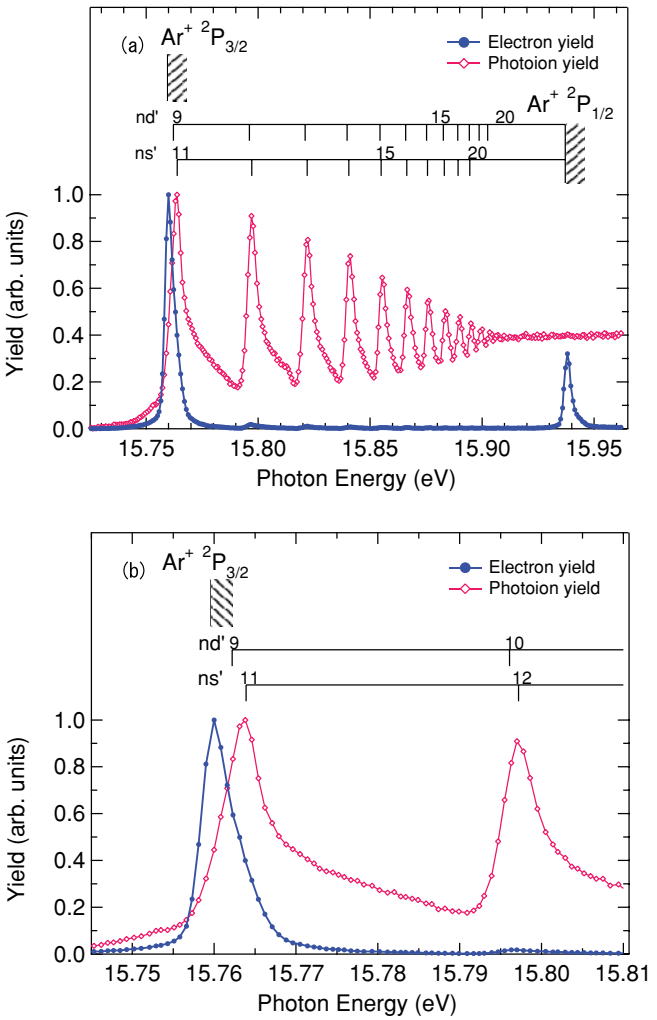

FIG. 3. (Color online) The electron yield spectrum and the photoion yield spectrum of Ar obtained simultaneously. (a) Photon energy range covering the spin-orbit splitting ionization thresholds and (b) close-up of the spectra around the first ionization threshold of Ar.

small, which lies 4 meV above the threshold. This shows the high selectivity for the low-energy photoelectrons in the present method.

The collection efficiency of the present apparatus for the photoelectrons as a function of the electron energy can be estimated from the electron yield spectrum of Fig. 3. The procedure for extracting the efficiency function is the same as used by Cvejanović and Reddish [46]. Following their procedure, the electron yield spectrum shown in Fig. 3 was fitted with $T(E)$, which is the function of photon energy E,

$$T(E) = \int_{-\infty}^{\infty} dE' \sigma_{\mathrm{Ar}}(E') F(E') G_{\mathrm{photon}}(E - E'), \qquad (2)$$

where $\sigma_{\mathrm{Ar}}(E)$ is the photoionizaiton cross section of Ar, $F(E)$ the efficiency function, and $G_{\mathrm{photon}}(E)$ the Gaussian function representing the energy width of the photon beam. In the present analysis, the photoionization cross section of Ar given by Maeda *et al.* [47] was employed. The analytic expression of the efficiency function can be approximated as [46]

$$F(E) = \frac{1}{a + (E - E_t)^b}, \qquad (3)$$

where E_t is the ionization threshold, the parameter a controls the half-width, and the b is the tail of the function. The energy width of the photon beam was determined by fitting the convoluted photoionization cross section of Ar, $\sigma_{\mathrm{Ar}}(E)$, with the Gaussian function, $G_{\mathrm{photon}}(E)$, to the photoion yield spectrum. In the present study, the energy width of the photon beam was estimated to be 2.7 meV.

In order to estimate the efficiency function, we have fitted Eq. (2) to the electron yield spectrum obtained at around the $Ar^+ {}^2P_{1/2}$ threshold and obtained the values of 0.87 and 1.6 for a and b, respectively. Since the partial photoionization cross section curve for $Ar^+ {}^2P_{1/2}$ state does not show complicated structure compared to that for the $Ar^+ {}^2P_{3/2}$ state, we chose the $Ar^+ {}^2P_{1/2}$ peak for the analysis.

In Fig. 4(a), the electron yield spectrum and the energy dependence of $T(E)$ obtained from the fitting are shown at around the $Ar^+ {}^2P_{3/2}$ threshold. The efficiency function $F(E)$ is shown in Fig. 4(b). As can be seen from Fig. 4(b), the collection efficiency for the photoelectrons of 1 meV kinetic

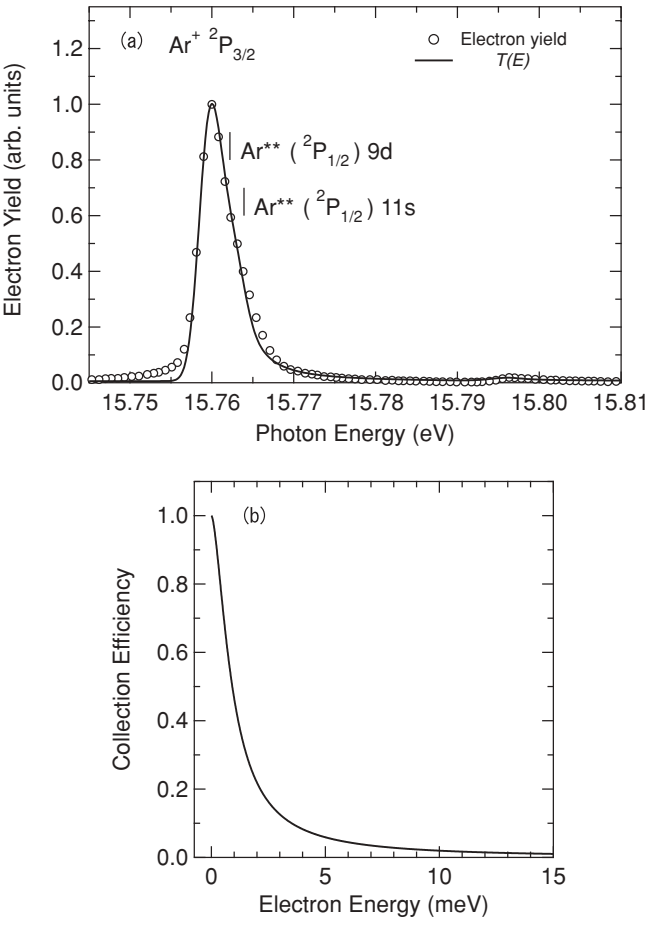

FIG. 4. (a) Electron yield spectrum and estimated energy dependence of $T(E)$. The solid curve represents $T(E)$ obtained by the fitting to the electron yield spectrum. (b) Collection efficiency curve $F(E)$ of the present setup.

energy reduces to less than a half, and for the photoelectrons produced from the autoionization of Ar^{**} $(4p^5{}^2P_{1/2})$ $11s'$, which have kinetic energy of 4 meV, the collection efficiency is about 10%.

The energy width of the electron beam in the present apparatus is determined by the product of the energy width of the ionization photon, the efficiency function $F(E)$, and photoionization cross section $\sigma_{Ar}(E)$. However, since the energy selectivity of the present technique is very high, as shown in Fig. 4(b), the energy distribution is dominated mainly by the efficiency function. Therefore, the present technique has the advantage that the energy width of the electron beam only slightly depends on the energy width of the ionization photon when the ionization photon width becomes wider than the energy width of the efficiency function.

D. Measurements of the total cross sections of electron scattering from krypton

The intensities of the electron beam, in the presence and absence of target gas (Kr, 99.99%), were recorded as a function of electron energy. During the measurements, the potentials supplied to the first lens system were kept constant while the second and third lens systems and the collision cell were controlled by programmable voltage supplies according to the electron energy of interest. Data acquisition was taken with a counting system controlled by a computer with dwell time of typically 1 s per channel for every scan. The pressure of the target gas in the collision cell was measured by a capacitance manometer.

The total cross section was obtained by using the attenuation law,

$$I(E) = I_0(E)\exp[-\sigma(E)nL], \tag{4}$$

where $I(E)$ and $I_0(E)$ are attenuated and unattenuated electron intensities obtained at the impact energy E, respectively, $\sigma(E)$ the total cross section, n the number density of the target gas, and L the effective path length of the electron in the target gas. In the present experiment, transmission of the electron beam (I/I_0) was kept above 50% in order to avoid inaccurate measurements for narrow structure known as the line saturation effect [48]. As pointed out by Roy *et al.* [49], the distortion of narrow structure would be significant in case of high pressure in transmission measurement, although the influence of the exponential in Eq. (4) can be neglected if the pressure is such that $\sigma(E)nL \ll 1$. In the present measurement, we took care of the pressure of the target to keep the transmission of the electron beam high enough so that the distortion was negligible.

The energy resolution was estimated by fitting the theoretical cross sections convoluted with a Gaussian function representing the resolution to those measured at around the Kr^- $(4p^5 5s^2{}^2P_{3/2})$ Feshbach resonance at 9.485 eV [40]. The electron energy was also calibrated against this resonance. The overall energy resolution of the present experiment was approximately 12 meV at around 10 eV. Details of the procedure are presented in the next section.

The pressure of target gas was measured by a capacitance manometer kept at a temperature of 318 K and the thermal transpiration correction with the empirical expression developed by Takaishi and Sensui [50] was made in the present measurement.

The effective path length of the electron in the target gas has been estimated based on the simulation of Mathur *et al.* [51] on the pressure variation effect near the aperture. It was found that the effective path length does not differ from the geometrical length of the collision cell within the experimental error for the present setup. In addition, we made a comparison of the measured total cross section for electron scattering from He with reported value [32]. Consequently, geometrical cell length was applied for Eq. (4) in the present study.

In the present method, stability of the intensity of the electron beam depends on the intensity and the energy of the photon beam. The stability of the photon beam intensity was achieved by the top-up operation of the Photon Factory facility that have been available in the recent operation [52]. Since the instability of the energy of the photon beam at small photon energy width causes fluctuation in the electron-beam intensity, we have used somewhat lower resolution for the photon beam during the measurement.

E. Contribution from forward-scattered electrons

In the attenuation method, the effect of the forward scattering, that is, incomplete discrimination against the electrons scattered at small angles with forward direction due to the finite angular resolution, contributes to the measured total cross section. In the present study, the contribution from the forward-scattered electrons was estimated as follows.

Incorporating the effect of the forward scattering, Eq. (4) can be rewritten as [53]

$$\ln\left(\frac{I_0(E)}{I(E)}\right) = nL\sigma(E) - n\int_0^L dz\int_0^{2\pi} d\phi\int_0^{\theta_{\max}(z,E)} \sin\theta d\theta \frac{d\sigma}{d\Omega}(E,\theta). \tag{5}$$

Here, θ is the angle between the beam axis and the direction of scattered electron and $\theta_{\max}(z,E)$ the maximum angle of the electrons which can be transmitted to the detector through the third lens system scattered at position z on the beam axis at impact energy E, and $d\sigma/d\Omega$ represents the elastic plus the inelastic differential cross sections.

Here we introduce $\langle\sigma_F(E)\rangle$ defined by

$$\langle\sigma_F(E)\rangle = \frac{1}{L}\int_0^L dz\int_0^{2\pi} d\phi\int_0^{\theta_{\max}(z,E)} \sin\theta d\theta \frac{d\sigma}{d\Omega}(E,\theta). \tag{6}$$

In order to calculate $\langle\sigma_F(E)\rangle$, $\theta_{\max}(z,E)$ have been estimated by calculating the trajectory of the electrons scattered at position z and energy E with the Charged Particle Optics computer program [54]. Since there is no data for the experimental differential cross sections at the very-low-energy region reported here, phase shifts reported in the theoretical work of McEachran and Stauffer [55] were applied for the calculation of $d\sigma/d\Omega$. The calculated results for $\langle\sigma_F(E)\rangle$ are listed in Table I together with the ratio of $\langle\sigma_F(E)\rangle$ to the measured total cross sections. As can be seen from Table I, the contribution from forward-scattered electrons is small in the present setup. Even near the Ramsauer-Townsend

TABLE I. Estimated values of partially integrated cross sections of forward scattering ($\langle\sigma_F(E)\rangle$) and the ratio of $\langle\sigma_F(E)\rangle$ to the measured total cross section of electron scattering from Kr.

Energy (eV)	$\langle\sigma_F(E)\rangle$ (10^{-20} m^2)	Ratio (%)
20.0	0.09	0.39
15.0	0.09	0.36
9.5	0.12	0.41
4.0	0.03	0.23
0.6	0.01	2.6
0.2	0.05	1.3
0.1	0.09	1.1
0.05	0.10	0.75
0.015	0.31	1.7

minimum, where the s-wave scattering diminishes, the ratio is less than 3%, which is fairly small compared to experimental uncertainty including the statistical errors. Therefore, the contribution from the forward-scattered electrons is negligible in the present results.

III. RESULTS AND DISCUSSION

A. Total cross section for electron scattering from krypton in the energy range from 14 meV to 20 eV

The total cross sections for electron scattering from Kr obtained in the energy range of 14 meV–20 eV in the present experiment are shown in Fig. 5. The numerical values for the selected points are also shown in Table II. The overall uncertainty in the cross section includes the statistical and systematic error. In Fig. 5, the well-known Ramsauer-Townsend minimum is seen at around 0.7 eV and the cross section rises gradually, reaching a maximum around 12 eV, and then decreases slowly with increasing electron energy. At 9.5 eV, the very sharp structure due to the Kr^- ($4p^5 5s^2\,^2P_{3/2}$) Feshbach resonance is seen on the total cross-section curve. A weak structure due to the Kr^- ($4p^5 5s^2\,^2P_{1/2}$) Feshbach resonance is also seen at 10.1 eV. Below the Ramsauer-Townsend minimum, the cross section increases rapidly with decreasing electron energy extending down to the energy range of cold electron collision regime.

In Fig. 5, previous experimental [28–33] and theoretical [55–58] total cross sections are also shown for comparison. In general, the present results agree with the reported experimental data. This shows that the present apparatus is performing adequately.

At around the highest measured energy, 20 eV, among the results of various experiments, the present results agree well with those of Szmytkowski *et al.* [32]. With decreasing energy, our data follow those of Szmytkowski *et al.* down to about 10 eV. From 10 and 5 eV, our data follow the results of Jost *et al.* [28], which are slightly larger than those of Szmytkowski *et al.* Below 5 eV, excellent agreement between the present results and those of Ferch *et al.* [29] is found.

In Fig. 6, a comparison of the total cross sections for electron scattering from Kr obtained in the present study with previously reported results is made in the energy range below 3 eV. Figure 6 shows that the cross-section values and the position of the Ramsauer-Townsend minimum of the present

TABLE II. The values of total cross sections for electron scattering from Kr obtained in the present work.

Energy (eV)	$\sigma(E)$ (10^{-20} m^2)
20.08	23.35(49)
19.08	23.43(49)
18.08	24.20(49)
17.08	24.61(49)
16.08	25.46(49)
15.08	26.37(49)
14.08	27.02(50)
13.08	27.63(50)
12.08	28.40(50)
11.08	28.35(50)
10.08	28.23(29)
9.08	27.68(50)
8.08	26.38(50)
7.08	23.50(50)
6.08	20.48(50)
5.08	16.50(50)
4.08	12.79(50)
3.06	8.09(23)
2.06	4.26(23)
1.563	2.47(22)
1.513	2.23(22)
1.463	2.10(22)
1.413	1.99(22)
1.363	1.87(22)
1.313	1.65(22)
1.263	1.52(22)
1.213	1.45(22)
1.163	1.28(22)
1.113	1.19(22)
1.063	1.02(22)
1.013	0.89(22)
0.963	0.85(22)
0.913	0.82(22)
0.863	0.75(22)
0.813	0.61(22)
0.763	0.53(22)
0.713	0.57(22)
0.663	0.55(22)
0.613	0.57(22)
0.563	0.67(22)
0.513	0.76(22)
0.463	0.94(22)
0.413	1.21(22)
0.363	1.47(22)
0.313	2.05(23)
0.263	2.76(23)
0.213	3.79(23)
0.163	4.90(29)
0.158	5.16(29)
0.153	5.31(29)
0.148	5.71(29)
0.143	5.85(29)
0.138	6.10(29)
0.133	6.25(29)
0.128	6.57(29)
0.123	6.79(30)
0.118	7.17(30)

TABLE II. *Continued.*

Energy (eV)	$\sigma(E)$ (10^{-20} m^2)
0.113	7.47(30)
0.108	7.61(30)
0.103	8.11(30)
0.098	8.63(30)
0.093	8.96(30)
0.088	9.23(31)
0.083	9.92(31)
0.078	10.29(30)
0.073	10.94(30)
0.068	11.92(31)
0.063	12.37(32)
0.062	12.00(55)
0.060	12.38(55)
0.058	12.69(56)
0.056	12.70(56)
0.054	13.02(57)
0.052	13.24(58)
0.050	13.65(60)
0.048	13.68(61)
0.046	13.66(62)
0.044	15.03(64)
0.042	14.09(65)
0.040	14.70(68)
0.038	15.61(70)
0.036	15.49(73)
0.034	15.45(77)
0.032	15.73(82)
0.030	15.87(89)
0.028	16.59(96)
0.026	14.68(104)
0.024	15.05(114)
0.022	17.65(126)
0.020	18.56(134)
0.018	16.45(145)
0.016	18.23(169)
0.014	20.22(229)

results agree well with those of Ferch *et al.* [29]. At energies below the minimum, the present results agree well with the cross sections obtained by Buckman and Lohmann [31] down to 175 meV. The cross sections obtained by Gus'kov *et al.* [33], which are the only available data in the literature below 175 meV, show a large discrepancy from the present results. The cross-section value at Ramsauer-Townsend minimum reported by Gus'kov *et al.* is about 20% smaller than the present results, and the cross-section value at 30 meV exceeds our results at about 50%.

In comparison with the theoretical results, the calculation by McEachran and Stauffer [55], using the polarized-orbital method with an adiabatic exchange approximation, reproduces the present results within the errors below 3 eV. In this calculation, the effects of the polarization potential and the accurate treatment of exchange have been employed. Further agreements in the value of the total cross sections and the energy position of the Ramsauer-Townsend minimum are given in the calculation by Mimnagh *et al.* [58], applying the polarized-orbital method under dynamic distortion effects.

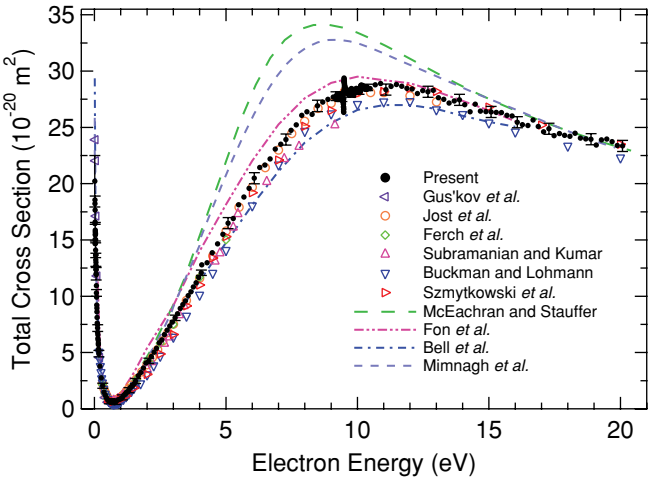

FIG. 5. (Color online) Total cross sections for electron scattering from krypton; •, present results. Also shown are experimental results of Gus'kov *et al.* [33], ◁; Jost *et al.* [28], ○; Ferch *et al.* [29], ◇; Subramanian and Kumar [30], △; Buckman and Lohmann [31], ▽; and Szmytkowski *et al.* [32], ▷; and theoretical results of McEachran and Stauffer [55], — — —; Fon *et al.* [56],–·· – ·· –; Bell *et al.* [57],–· – · –; and Mimnagh *et al.* [58], – – – –.

Moreover, this calculation reproduces the present results below the Ramsauer-Townsend minimum, and especially below 50 meV. However, both of the polarized-orbital methods show disagreement against the present results in the preceding energy range. The *R*-matrix calculation by Bell *et al.* [57], which takes into account a ^1P pseudostate as the static dipole polarizability of the target atom, also reproduces the present results from 200 meV to 3 eV, including the value of the cross section and the position of the minimum. The cross sections calculated by Fon *et al.* [56] with the *R*-matrix method are somewhat higher than our results.

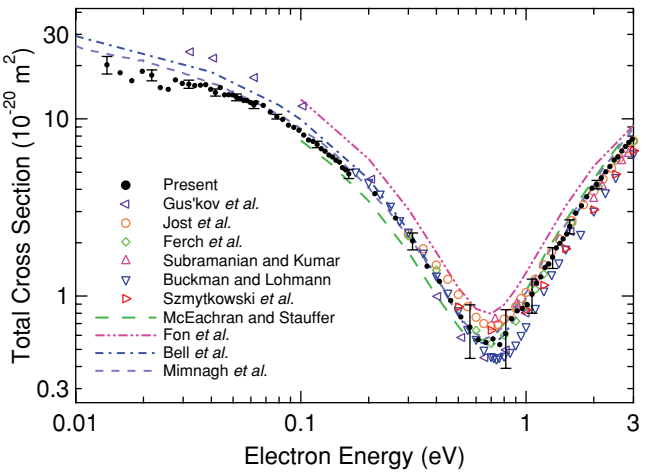

FIG. 6. (Color online) Total cross sections for electron scattering from krypton in the energy range below 3 eV; •, present results. Also shown are experimental results of Gus'kov *et al.* [33], ◁; Jost *et al.* [28], ○; Ferch *et al.* [29], ◇; Subramanian and Kumar [30], △; Buckman and Lohmann [31], ▽; and Szmytkowski *et al.* [32], ▷; and theoretical results of McEachran and Stauffer [55], — — —; Fon *et al.* [56], – ·· – ·· –; Bell *et al.* [57], – · – · –; and Mimnagh *et al.* [58] – – – –.

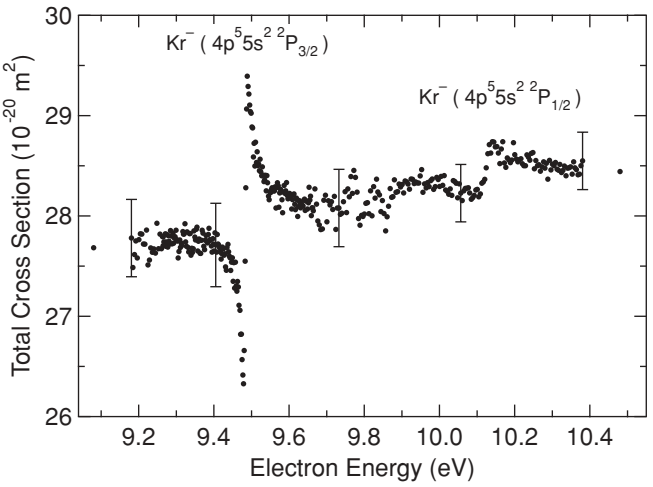

FIG. 7. Total cross sections for electron scattering from krypton at around the Kr^- $(4p^5 5s^{2\,2}P_{3/2})$ and the Kr^- $(4p^5 5s^{2\,2}P_{1/2})$ Feshbach resonances.

B. Total cross section at around the Kr^- $(4p^5 5s^{2\,2}P_{3/2})$ and Kr^- $(4p^5 5s^{2\,2}P_{1/2})$ Feshbach resonances and the resolution of the present apparatus

The Kr^- $(4p^5 5s^{2\,2}P_{3/2})$ and the Kr^- $(4p^5 5s^{2\,2}P_{1/2})$ Feshbach resonances have been studied extensively by transmission measurements [34–36] and angular differential cross-section measurements [21,37–40]. On the other hand, the total cross sections for these resonances have not been reported previously. In Fig. 7, the total cross sections for electron scattering from Kr obtained in the energy region of 9.2–10.4 eV are shown. The narrow resonant structure due to the $^2P_{3/2}$ Feshbach resonance is clearly seen in the figure. The structure due to the $^2P_{1/2}$ resonance is also observed, which is slightly broader than that of the $^2P_{3/2}$ resonance. The $^2P_{1/2}$ resonance appears above the energy of the lowest excited state of Kr $(4p^5 5s,\ J=2)$ at 9.915 eV and the second excited state Kr $(4p^5 5s,\ J=1)$ at 10.032 eV [37]. Therefore, the higher lying $^2P_{1/2}$ resonance can decay into both of these states in addition to the ground state, resulting in broader width of the $^2P_{1/2}$ resonance compared to the $^2P_{3/2}$ resonance. It is also found that the intensity of the $^2P_{1/2}$ resonance is smaller than half of that of $^2P_{3/2}$ resonance, as is expected from the statistical weight. Since the phase shifts for the elastic and the inelastic channels would not be the same for each other, the intensity ratio of the $^2P_{1/2}$ resonance to the $^2P_{3/2}$ resonance might be smaller than that expected from the statistical weight.

An analysis of the resonant structure was performed in order to estimate the resolution with a model curve obtained from the partial wave description for spin-dependent scattering convoluted with a Gaussian function of the width corresponding to the energy resolution of the experiment. The calibration of the experimental energy scale was also obtained in the analysis, using the energy position of the resonance.

In the presence of significant spin-orbit coupling, the integral electron scattering cross sections for elastic scattering is given by

$$\sigma(E) = 2\pi \int_0^\pi (|f(\theta,E)|^2 + |g(\theta,E)|^2\, x)\, \sin\theta d\theta, \qquad (7)$$

where the direct and exchange amplitude $f(\theta,E)$ and $g(\theta,E)$ are given by partial-wave sums as follows [18,59]:

$$f(\theta,E) = \frac{1}{2ik}\sum_l^\infty ((l+1)\{\exp[2i\delta_l^+(k)] - 1\} + l\{\exp[2i\delta_l^-(k)] - 1\})P_l(\cos\theta), \qquad (8)$$

$$g(\theta,E) = \frac{1}{2ik}\sum_l^\infty \{\exp[2i\delta_l^+(k)] - \exp[2i\delta_l^-(k)]\}P_l^1(\cos\theta). \qquad (9)$$

Here k is the wave number of electrons related to the collision energy E, $P_l(\cos\theta)$ the standard Legendre polynomials, $P_l^1(\cos\theta)$ $(L \geqslant 1)$ an associated Legendre polynomial, while $\delta_l^+(k)$ and $\delta_l^-(k)$ represent the phase shifts in the partial wave with total electronic angular momenta of $j^+ = l + 1/2$ and $j^- = l - 1/2$, respectively. For the resonance states below the first excited state of the atom, the variation in the cross section arises from rapid changes of the phase shift, $\delta_l^+(k)$ or $\delta_l^-(k)$ of the resonance partial wave ($l = 1$ for the present resonances), by a value of π. In the energy region close to a resonance at an energy E_r, the phase shift changes according to the expression

$$\delta_l^\pm(E) = \delta_l^{0\pm}(E) + \cot^{-1}\frac{E - E_r^\pm}{\Gamma^\pm/2}, \qquad (10)$$

where Γ is the half-width (natural width) of the resonance and $\delta_l^{0\pm}(E)$ the potential (nonresonant) scattering phase shift, which varies only slowly with electron energy.

Since the electron scattering cross section $\sigma(E)$ is the sum of a direct scattering $\sigma_{\rm direct}(E)$ and resonant scattering $\sigma_{\rm res}(E)$, the difference between the total cross section and the cross section due to direct scattering is the cross section due to the resonance. Here let us introduce the cross section $\sigma_{\rm res}(E)$ due to the resonant scattering given by

$$\begin{aligned}\sigma_{\rm res}(E) &= \sigma(E) - \frac{\pi}{k^2}\sum_l^\infty \{4(l+1)\sin^2\delta_l^{0+} + 4l\sin^2\delta_l^{0-}\} \\ &= \frac{8\pi}{k^2}\left\{\sin^2\left(\delta_1^{0+} + \cot^{-1}\frac{E - E_{3/2}}{\Gamma_{3/2}/2}\right) - \sin^2\delta_1^+\right\} \\ &\quad + \frac{4\pi}{k^2}\left\{\sin^2\left(\delta_1^{0-} + \cot^{-1}\frac{E - E_{1/2}}{\Gamma_{1/2}/2}\right) - \sin^2\delta_1^-\right\}.\end{aligned} \qquad (11)$$

In the present analysis, the nonresonant background due to the direct scattering has been approximated by a fourth-order polynomial and subtracted from the measured cross-section curve.

The resulting curve representing the resonant scattering is shown together with the fitted curve in Fig. 8. The fitted curve has been obtained by employing the energy-dependent phase shifts extracted from interpolation of the theoretical values of Sienkiewicz and Baylis at 7.0 and 10.0 eV [60] and the resonance width of 3.5 meV and the resonance energy of 9.485 eV reported by Zubek *et al.* [40]. As a result of the present analysis, the energy resolution of the present apparatus has been estimated to be 11 meV, apart from the Doppler broadening of 4.2 meV.

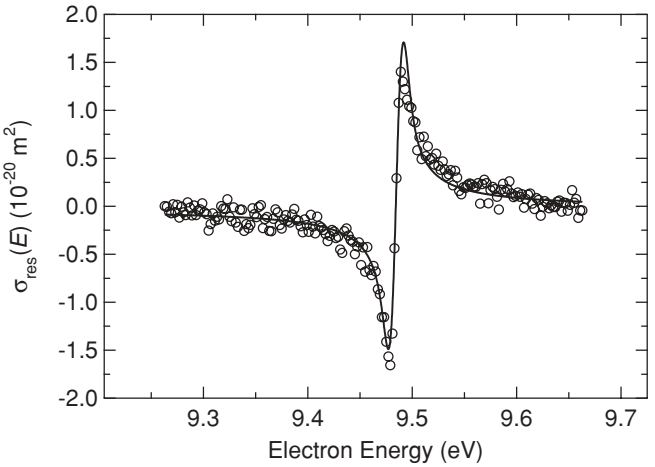

FIG. 8. The cross sections due to the Kr^- $(4p^5 5s^2\,^2P_{3/2})$ Feshbach resonance. The solid curve shows the best fit for the resonant cross sections obtained by the fitting the calculated $\sigma_{res}(E)$ (see text).

The energy resolution obtained by this estimation seems rather wider than that expected from the collection efficiency curve $F(E)$ of the photoelectrons in Fig. 4(b). Since the size of the ionizing photon beam may contribute to the broadening of the electron energy, we have measured the total cross section around the resonance with increasing the size of the photon beam to 2 mm. The energy width of the electron beam, however, did not change significantly. This shows that the energy width of the electron beam was not determined by the photoelectron source, but rather by the surface potential variations inside the collision cell due to the work function of the materials and the shape of the electrode. Here we conclude that the present method of applying the penetrating field technique for the photoelectron source has certain potential for the electron collision experiment over the wide energy range, that is, a few meV to a few tens of eV, with high energy resolution.

IV. CONCLUSION

An experimental technique has been developed to measure total cross section for electron scattering over the wide energy range down to the cold electron collision regime. The present technique makes it possible to perform high energy resolution experiments by employing the penetrating field technique together with the threshold photoionizaion of atoms by the SR. The high energy selectivity of the present photoelectron source was confirmed by measuring the electron yield spectrum. The collection efficiency for the photoelectrons of 1 meV kinetic energy reduces to less than a half in the present method. Due to this high energy selectivity of the present technique, together with the reduced strength of the photoelectron-extracting field applied at the photoionizaiton region, the present method overcomes the trade-off problem between the resolution and the intensity of the electron beam.

In the present study, the total cross section of electron scattering from krypton is obtained in the energy range from 14 meV to 20 eV at an electron energy width of 11 meV. Although the energy resolution was wider than expected, high resolution was obtained compared to the conventional technique using a hot filament for the electron source.

The total cross sections for electron scattering from krypton obtained in the present study agree well with the measurements of Buckman and Lohmann [31] from 175 meV to at around 0.7 eV, where the Ramsauer-Townsend minimum occurs. Excellent agreement with the results by Ferch *et al.* [29] was found for the cross-section values and the position of the Ramsauer-Townsend minimum. The present cross-section values also agree well with those by Ferch *et al.* [29] up to 5 eV. On the other hand, the cross-section values reported by Gus'kov *et al.* [33] at the very-low-energy region turned out to be too large. Fairly good agreements between the present results and previous theoretical ones are found at very low energy. Total cross sections at around the Kr^- $(4p^5 5s^2\,^2P_{3/2})$ and the Kr^- $(4p^5 5s^2\,^2P_{1/2})$ Feshbach resonances were also obtained and reported. The results also demonstrate that the present technique utilizing the described photoelectron source has been developed to be a reliable method for high-resolution measurements in a wide energy range down to the cold electron collision regime.

ACKNOWLEDGMENTS

This work was supported by the Grant-in-Aid for Scientific Research (C) (Grants No. 18540390 and No. 20540387), the Japan Society for the Promotion of Science, and a Cooperative Research Grant from National Institute for Fusion Science, Japan (Grant No. NIFS06KOAP014). This work has been carried out under the approval of Photon Factory Program Advisory Committee under Proposals No. 2006G233 and No. 2008G639.

[1] C. Ramsauer, Ann. Phys. (Leipzig) **66**, 546 (1922).
[2] J. S. Townsend and V. A. Bailey, Philos. Mag. **43**, 593 (1922).
[3] G. J. Schulz, Rev. Mod. Phys. **45**, 378 (1973).
[4] G. J. Schulz, Rev. Mod. Phys. **45**, 423 (1973).
[5] M. Allan, Phys. Rev. Lett. **87**, 033201 (2001).
[6] J. Ferch, W. Raith, and K. Schröder, J. Phys. B **13**, 1481 (1980).
[7] S. J. Buckman and B. Lohmann, J. Phys. B **19**, 2547 (1986).
[8] A. C. Gallagher and G. York, Rev. Sci. Instrum. **45**, 662 (1974).
[9] R. E. Kennerly, R. J. Van Brunt, and A. C. Gallagher, Phys. Rev. A **23**, 2430 (1981).
[10] A. Chutjian and S. H. Alajajian, Phys. Rev. A **31**, 2885 (1985).
[11] A. Chutjian, A. Garscadden, and J. M. Wadehra, Phys. Rep. **264**, 393 (1996).
[12] D. Klar, M.-W. Ruf, and H. Hotop, Meas. Sci. Technol. **5**, 1248 (1994).
[13] J. M. Weber, E. Leber, M.-W. Ruf, and H. Hotop, Eur. Phys. J. D **7**, 587 (1999).
[14] A. Schramm, J. M. Weber, J. Kreil, D. Klar, M.-W. Ruf, and H. Hotop, Phys. Rev. Lett. **81**, 778 (1998).
[15] A. Schramm, I. I. Fabrikant, J. M. Weber, E. Leber, M.-W. Ruf, and H. Hotop, J. Phys. B **32**, 2153 (1999).

[16] H. Hotop, M.-W. Ruf, M. Allan, and I. I. Fabrikant, Adv. At. Mol. Opt. Phys. **49**, 85 (2003).
[17] A. Gopalan, J. Bömmels, S. Götte, A. Landwehr, K. Franz, M.-W. Ruf, H. Hotop, and K. Bartschat, Eur. Phys. J. D **22**, 17 (2003).
[18] J. Bömmels, K. Franz, T. H. Höffmann, A. Gopalan, O. Zatsarinny, K. Bartschat, M.-W. Ruf, and H. Hotop, Phys. Rev. A **71**, 012704 (2005).
[19] K. Franz, T. H. Hoffmann, J. Bömmels, A. Gopalan, G. Sauter, W. Meyer, M. Allan, M.-W. Ruf, and H. Hotop, Phys. Rev. A **78**, 012712 (2008).
[20] T. H. Hoffmann, M. Allan, K. Franz, M.-W. Ruf, H. Hotop, G. Sauter, and W. Meyer, J. Phys. B **42**, 215202 (2009).
[21] T. H. Hoffmann, M.-W. Ruf, H. Hotop, O. Zatsarinny, K. Bartschat, and M. Allan, J. Phys. B **43**, 085206 (2010).
[22] D. Field, J. P. Ziesel, P. M. Guyon, and T. R. Govers, J. Phys. B **17**, 4565 (1984).
[23] D. Field, D. W. Knight, G. Mrotzek, J. Randell, S. L. Lunt, J. B. Ozenne, and J. P. Ziesel, Meas. Sci. Technol. **2**, 757 (1991).
[24] D. Field, S. L. Lunt, and J.-P. Ziesel, Acc. Chem. Res. **34**, 291 (2001).
[25] D. Field, N. C. Jones, S. L. Lunt, and J.-P. Ziesel, Phys. Rev. A **64**, 022708 (2001).
[26] N. C. Jones, D. Field, S. L. Lunt, and J.-P. Ziesel, Phys. Rev. A **78**, 042714 (2008).
[27] S. Cvejanović and F. H. Read, J. Phys. B **7**, 1180 (1974).
[28] K. Jost, P. G. F. Bisling, F. Eschen, M. Felsmann, and L. Walther, in *Abstracts of Contributed Papers, 13th International Conference on the Physics of Electronic and Atomic Collisions, Berlin, 1983*, edited by J. Eichler, W. Fritsch, I. V. Hertel, N. Stolterfoht, and U. Wille (Berlin, Germany, 1983), p. 91. (The corrected cross-section data reported in Ref. [29] are cited here.)
[29] J. Ferch, F. Simon, and G. Strakeljahn, in *Abstracts of Contributed Papers, 15th International Conference on the Physics of Electronic and Atomic Collisions, Brighton, 1987*, edited by J. Geddes, H. B. Gilbody, A. E. Kingston, C. J. Latimer, and H. J. R. Walters (Brighton, UK, 1987), p. 132.
[30] K. P. Subramanian and V. Kumar, J. Phys. B **20**, 5505 (1987).
[31] S. J. Buckman and B. Lohmann, J. Phys. B **20**, 5807 (1987).
[32] C. Szmytkowski, K. Maciąg, and G. Karwasz, Phys. Scr. **54**, 271 (1996).
[33] Yu. K. Gus'kov, R. V. Savvov, and V. A. Slobodyanyuk, Sov. Phys.-Tech. Phys. **23**, 167 (1978).
[34] G. J. Schulz, Phys. Rev. **136**, A650 (1964).
[35] L. Sanche and G. J. Schulz, Phys. Rev. A **5**, 1672 (1972).
[36] C. E. Kuyatt, J. A. Simpson, and S. R. Mielczarek, Phys. Rev. **138**, A385 (1965).
[37] N. Swanson, J. W. Cooper, and C. E. Kuyatt, Phys. Rev. A **8**, 1825 (1973).
[38] A. Weingartshofer, K. Willmann, and E. M. Clarke, J. Phys. B **7**, 79 (1974).
[39] D. Dubé, D. Tremblay, and D. Roy, Phys. Rev. A **47**, 2893 (1993).
[40] M. Zubek, B. Mielewska, J. Channing, G. C. King, and F. H. Read, J. Phys. B **32**, 1351 (1999).
[41] K. Ito, Y. Morioka, M. Ukai, N. Kouchi, Y. Hatano, and T. Hayaishi, Rev. Sci. Instrum. **66**, 2119 (1995).
[42] G. C. King, M. Zubek, P. M. Rutter, and F. H. Read, J. Phys. E **20**, 440 (1987).
[43] R. I. Hall, A. McConkey, K. Ellis, G. Dawber, L. Avaldi, M. A. MacDonald, and G. C. King, Meas. Sci. Technol. **3**, 316 (1992).
[44] J. A. R. Samson, Rev. Sci. Instrum. **40**, 1174 (1969).
[45] K. Radler and J. Berkowitz, J. Chem. Phys. **70**, 221 (1979).
[46] S. Cvejanović and T. J. Reddish, J. Phys. B **28**, L1 (1995).
[47] K. Maeda, K. Ueda, and K. Ito, J. Phys. B **26**, 1541 (1993).
[48] W. F. Chan, G. Cooper, and C. E. Brion, Phys. Rev. A **44**, 186 (1991).
[49] D. Roy, A. Delage, and J.-D. Carette, J. Phys. E **8**, 109 (1984).
[50] T. Takaisi and Y. Sensui, Trans. Faraday Soc. **59**, 2503 (1963).
[51] B. P. Mathur, J. E. Field, and S. O. Colgate, Phys. Rev. A **11**, 830 (1975).
[52] H. Takaki, N. Nakamura, Y. Kobayashi, K. Harada, T. Miyajima, A. Ueda, S. Nagahashi, M. Shimada, T. Obina, and T. Honda, Phys. Rev. ST Accel. Beams **13**, 020705 (2010).
[53] H. J. Blaauw, R. W. Wagenaar, D. H. Barends, and F. J. de Heer, J. Phys. B **13**, 359 (1980).
[54] Charged Particle Optics programs [http://www.electronoptics.com].
[55] R. P. McEachran and A. D. Stauffer, J. Phys. B **17**, 2507 (1984).
[56] W. C. Fon, K. A. Berrington, and A. Hibbert, J. Phys. B **17**, 3279 (1984).
[57] K. L. Bell, K. A. Berrington, and A. Hibbert, J. Phys. B **21**, 4205 (1988).
[58] D. J. R. Mimnagh, R. P. McEachran, and A. D. Stauffer, J. Phys. B **26**, 1727 (1993).
[59] N. F. Mott and H. S. W. Massey, *The Theory of Atomic Collisions* (Oxford University Press, Oxford, 1965).
[60] J. E. Sienkiewicz and W. E. Baylis, J. Phys. B **24**, 1739 (1991).